BIOCHEMISTRY
including biophysical chemistry & molecular biology
Article

Biochemistry **2010,** *49,* 7733–7747 7733
DOI: 10.1021/bi100780t

Functional Analysis, Overexpression, and Kinetic Characterization of Pyruvate Kinase from Methicillin-Resistant *Staphylococcus aureus*[†]

Roya Zoraghi,[‡] Raymond H. See,[‡,⊥] Huansheng Gong,[‡] Tian Lian,[‡] Rick Swayze,[‡] B. Brett Finlay,[§,∥] Robert C. Brunham,[‡,⊥] William R. McMaster,[‡,∥] and Neil E. Reiner*[,‡,∥]

[‡]*Division of Infectious Diseases, Department of Medicine,* [§]*Department of Biochemistry and Molecular Biology,* [∥]*Department of Microbiology and Immunology, and* [⊥]*Centre for Disease Control, University of British Columbia, Vancouver, Britsih Columbia, Canada V5Z 3J5*

Received May 18, 2010; Revised Manuscript Received July 29, 2010

ABSTRACT: Novel antimicrobial targets are urgently needed to overcome rising antibiotic resistance of important human pathogens including methicillin-resistant *Staphylococcus aureus* (MRSA). Here we report the essentiality and kinetic properties of MRSA pyruvate kinase (PK). Targetron-mediated gene disruption demonstrated PK is essential for *S. aureus* growth and survival, suggesting that this protein may be a potential drug target. The presence of the *pfk* (6-phosphofructokinase)−*pyk* operon in MRSA252, and the nonessential nature of PFK shown by targetron, further emphasized the essential role of PK in cell viability. The importance of PK in bacterial growth was confirmed by showing that its enzymatic activity peaked during the logarithmic phase of *S. aureus* growth. PK from *Staphylococcus* and several other species of bacteria have an extra C-terminal domain (CT) containing a phosphoenolpyruvate (PEP) binding motif. To elucidate the possible structure and function of this sequence, the quaternary structures and kinetic properties of the full-length MRSA PK and truncated MRSA PK lacking the CT domain were characterized. Our results showed that (1) MRSA PK is an allosteric enzyme with homotetramer architecture activated by AMP or ribose 5-phosphate (R5P), but not by fructose 1,6-bisphosphate (FBP), which suggests a different mode of allosteric regulation when compared with human isozymes, (2) the CT domain is not required for the tetramerization of the enzyme; homotetramerization occurred in a truncated PK lacking the domain, (3) truncated enzyme exhibited high affinity toward both PEP and ADP and exhibited hyperbolic kinetics toward PEP in the presence of activators (AMP and R5P) consistent with kinetic properties of full-length enzyme, indicating that the CT domain is not required for substrate binding or allosteric regulation observed in the holoenzyme, (4) the kinetic efficiency ($k_{cat}/S_{0.5}$) of truncated enzyme was decreased by 24- and 16-fold, in ligand-free state, toward PEP and ADP, respectively, but was restored by 3-fold in AMP-bound state, suggesting that the sequence containing the CT domain (Gly^{473}−Leu^{585}) plays a substantial role in enzyme activity and comformational stability, and (5) full-length MRSA PK activity was stimulated at low concentrations of ATP (e.g., 1 mM) and inhibited by inorganic phosphate and high concentrations of FBP (10 mM) and ATP (e.g., >2.5 mM), whereas for truncated enzyme, stimulation at low concentrations of ATP was lost. These findings suggest that the CT domain is involved in maintaining the specificity of allosteric regulation of MRSA PK by AMP, R5P, and ATP. The CT extension also encodes a protein domain with homology to enzyme I of the *Escherichia coli* sugar−PTS system, suggesting that MRSA PK may also exert an important regulatory role in sugar transport metabolism. These findings yield new insights into MRSA PK function and mode of allosteric regulation which may aid in the development of clinically important drugs targeting this enzyme and further define the role of the extra C-terminal domain in modulating the enzyme's activity.

Pyruvate kinase (PK)[1] (EC 2.7.1.40), a final-stage enzyme in glycolysis, catalyzes the transfer of a phosphoryl group from phosphoenolpyruvate (PEP) to adenosine diphosphate (ADP), generating the substrates ATP and pyruvate for anaerobic and aerobic metabolism (*1*−*6*). This reaction is essentially irreversible in vivo ($K_{eq} = 10^3$ to 10^4) and appears to be one of the major control points for the regulation of the glycolytic flux. In addition, both substrate and products of this reaction feed into a number of energetic and biosynthetic pathways, placing PK at a primary metabolic intersection. The X-ray crystal structures of several PKs from different species (e.g., *Escherichia coli*, *Leishmania mexicana*, *Bacillus stearothermophilus*, cat, rabbit muscle, human erythrocyte, and yeast) revealed a high degree of structural homology in the general PK topology (*2*−*5*, *7*). PKs exist as homotetramers of identical subunits of ∼50−60 KDa depending on species, each consisting of three to four domains: A, B, C, and N-terminal domains (Figure 1). The N-terminal helical domain is

[†]This work was supported by funding from Genome Canada, Genome British Columbia, Vancouver General Hospital and UBC Hospital Foundation, and SARS Accelerated Vaccine Initiative to the PRoteomics for Emerging PAthogen REsponse (PREPARE) Project. Computer equipment in PREPARE Project's Computational Genomics research was also supported by in-kind contribution from IBM Healthcare and Life Sciences.

*Corresponding author. E-mail: ethan@interchange.ubc.ca. Tel: 604-875-4011. Fax: 604-875-5654.

[1]Abbreviations: *S. aureus*, *Staphylococcus aureus*; MRSA, methicillin-resistant *S. aureus*; PK, pyruvate kinase; CT, extra C-terminal domain; PEP, phosphoenolpyruvate; R5P, ribose 5-phosphate; FBP, fructose 1,6-bisphosphate; AMP, adenosine 5′-monophosphate; ADP, adenosine diphosphate; PFK, 6-phosphofructokinase; F26BP, fructose 2,6-diphosphate; HPr, phosphoryl carrier protein; PPDK, orthophosphate dikinase; PTS, phosphotransferase system; EI, enzyme I.

Published on Web 07/30/2010

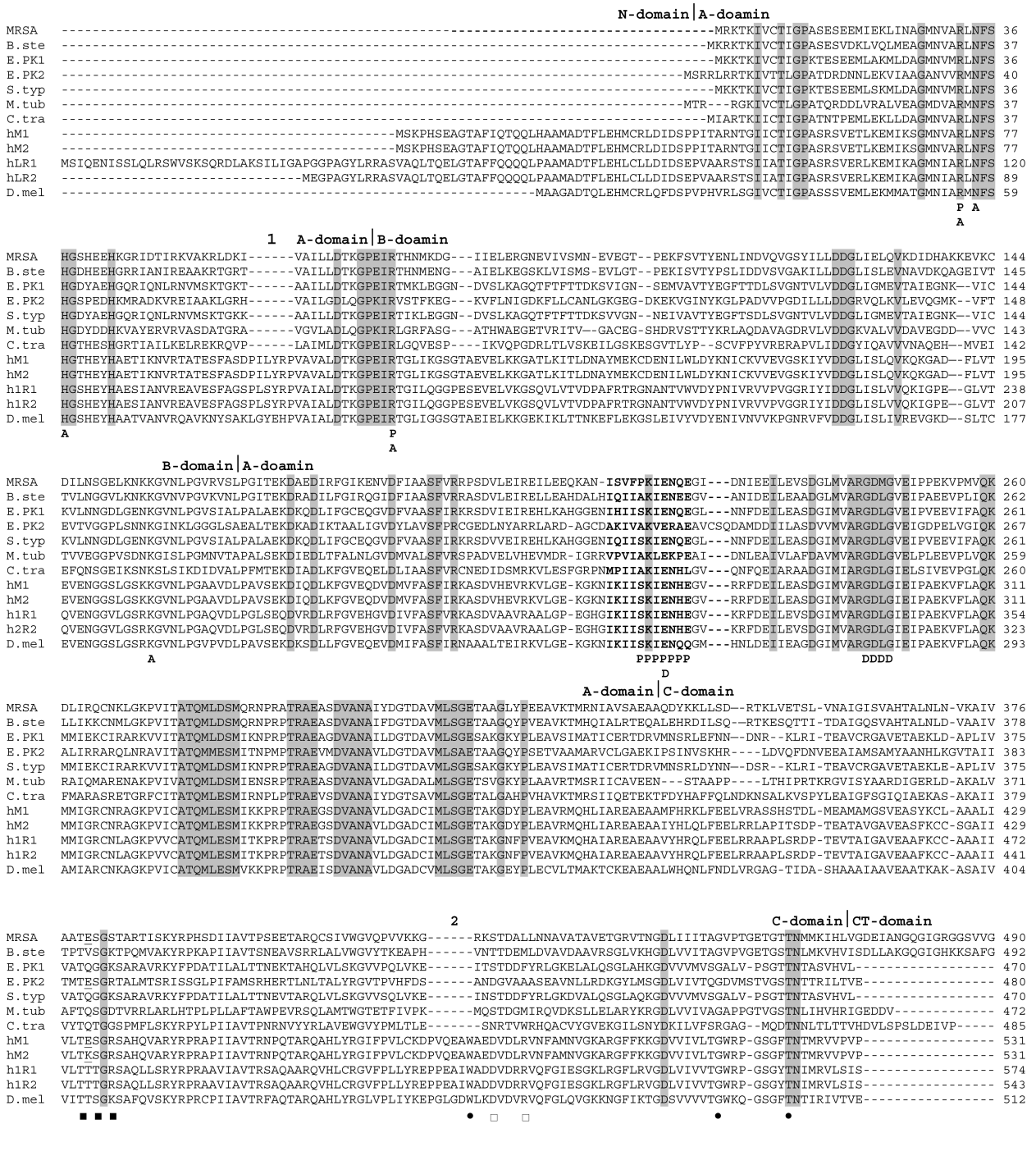

FIGURE 1: Amino acid sequence alignment of MRSA PK with pyruvate kinases from other species. Accession numbers: MRSA, (this study; YP_041163.1); B.ste, *B. stearothermophilus* (BAA02406); E.PK1, *E. coli* PK1 (NP_288110.1); E.PK2, *E. coli* PK2 (ACT72239); S.typ, *S. typhimurium* (NP_460343.1); M.tub, *M. tuberculosis* (NP_216133.1); C.tra, *C. trachomatis* (NP_219839.1); hM1, human M1 (NP_872270.1); hM2, human muscle isozyme M2 (NP_002645.3); hLR1, human LR1 (NP_000289.1); hLR2, human LR2 (NP_870986.1); D.mel, *D. melanogaster* (NP_732723.1). The 3D domains (N/A/B/C/CT) are indicated by vertical lines. Bold AAs indicate PK signature sequences. Thick cursive letters A, P, and D indicate ATP, PEP, and divalent cation binding sites, respectively. The binding sites of the sugar, 1-phosphate, and 6-phosphate moieties of FBP are indicated by closed circles, open squares, and closed squares, respectively. Numbers 1 and 2 indicate deletions in the MRSA sequence compared to the host homologues. According to the percent conservation, columns of residues having 100% conservation are shaded.

absent in prokaryotic PKs and can be removed from human erythrocyte PK with no effect on its stability or activity (*8*). The A domain with β/α-barrel topology is located between the B (with β-barrel structure) and C (with α/β topology) domains. The active site lies at the interface of the A and B domains in each of the four subunits while the binding site for allosteric effector appears to be located at the C domain (Figure 1) (*2*, *3*).

While there are four mammalian PK isozymes, M1, M2, L (liver), and R (red blood cell), with different primary structures, kinetic properties, and tissue distributions to satisfy the metabolic

requirements of various tissues, most bacteria and lower eukaryotes have only one PK isoenzyme; only a few bacterial species (i.e., *E. coli* and *Salmonella typhimurium*) have two isoenzymes.

PK is subject to various types of regulation, such as tissue-specific isozyme distribution, phosphorylation−dephosphorylation, and allosteric regulation, to regulate the switching between glycolysis and gluconeogenesis (*9*). Allosteric regulation, in particular, provides mechanisms for tight modulation of PK enzymes. All known PKs (except mammalian muscle M1 isoform) exhibit an inactive/active reversible association depending on allosteric activation by PEP and one or more allosteric effector(s) whose precise chemical nature depends on the source of enzyme.

Fructose 1,6-bisphosphate (FBP) acts as a potent allosteric activator of a number of PKs of different origin (e.g., mammalian M2, L and R isozymes, yeast PK, and some bacterial PKs) (*1*, *10*, *11*), whereas in trypanosomatid protozoans *L. mexicana* and *Chlamydia trachomatis* the allosteric activator is fructose 2,6-diphosphate (F26BP) (*5*, *12*, *13*). The relationship of structure to this allosteric regulation of PK activity is not fully understood. However, it was shown recently that the transition between inactive T-state and active R-state involved a symmetrical 6° rigid-body rocking motion of the A- and C-domain cores in each of the four subunits. This also involved the formation of eight essential salt-bridge locks across the C−C interface that provided tetramer rigidity and a 7-fold increase in enzyme activity (*14*).

PKs have been isolated and characterized from numerous bacterial species (e.g., *E. coli* (*15*), *B. stearothermophilus* (*16*), *Pseudomonas citronellolis* (*17*), *Streptococcus lactis* (*18*), *Lactobacillus bulgaricus* (*19*), *Mycobacterium smegmatis* (*20*), and *C. trachomatis* (*13*). However, due to their general instability, bacterial enzymes have not been extensively studied. We know, nevertheless, that similar to eukaryotic PKs bacterial PKs demonstrate tight allosteric control by a variety of metabolite effectors. In *E. coli*, PK1 is inducible and activated by FBP, whereas the enzymatic activity of PK2 is constitutive and activated by AMP and ribose 5-phosphate (R5P) (*21*). The latter may play an essential role in the production of ATP under anaerobic conditions.

PKs has recently been drawing a lot of attention as a novel target for antitrypanosomal, antileishmania, antimalaria, and anticancer drugs (*22*−*26*). This has particular relevance, since the high prevalence of multidrug-resistant organisms such as methicillin-resistant *Staphylococcus aureus* (MRSA) has generated an intensive search for alternative targets for development of new antimicrobials. Potential target genes should be essential for bacterial viability and pathogenesis (*27*). Until now, no studies of this crucial metabolic enzyme have been carried out for *S. aureus*, leaving its structural, kinetic, and regulatory properties unknown. The current series of experiments were designed to address these deficiencies. Our results show that *S. aureus* PK carries out an absolutely essential function for survival of this key Gram-positive pathogen. Moreover, we found that PK enzymatic activity increases during the exponential phase of *S. aureus* growth. These data, together with the high level sequence and likely structural divergence between bacterial and mammalian PKs, indicate that PK is a potential novel antibacterial target. Consequently, we expressed *S. aureus* PK as an active recombinant enzyme and, for the first time, report a comprehensive functional, structural, and biochemical characterization of the MRSA PK protein. PKs from various species of staphylococci and several other bacteria (e.g., *Bacillus* sp. and *Listeria* sp.) have a conserved PEP utilizer superfamily domain as an extra C-terminal (CT) sequence, the role of which is not yet understood (*6*, *16*, *28*, *29*). We characterized MRSA PK as the second CT-containing PK studied to date. We also extensively defined the contribution of the CT domain to the holoenzyme structure, function, and mode of regulation by studying the kinetic properties, regulatory behavior, and biophysical properties of a truncated MRSA PK mutant in which the CT domain was deleted. The results reported below improve our understanding of the control mechanisms governing primary carbon metabolism in *S. aureus*. They also provide insights into the functional features and mechanisms of regulation of *S. aureus* PK and its significance as a potential anti-MRSA drug target.

MATERIALS AND METHODS

Bacterial Strains and Plasmids. Epidemic methicillin-resistant *S. aureus* (MRSA) strain sequenced at Sanger Centre, U.K. (Sanger 252 NRS71), and *S. aureus* RN4220 (NCTC8325 NRS144) were obtained from NARSA (The network on antimicrobial resistance in *S. aureus*). The staphylococcal plasmid pNL9162 used for PK essentiality evaluation was from Sigma-Aldrich.

S. aureus Pyk Gene Inactivation Using Targetron Technology. PK gene (*pyk* 1755 bp) was disrupted independently at three different target sites (312, 357, and 390 bp) by insertion of a group II intron in the sense orientation relative to *pyk* transcription using targetron technology. Attempts were also made to disrupt PK gene by insertion of the intron in the antisense orientation (77 bp). The *pyk*−targetron target fragments of 350 bp were amplified by three specific primers (PK-IBS, PK-EBS1d, and PK-EBS2) for each construct, according to the protocol of the Targetron gene knockout system kit (Sigma-Aldrich, St. Louis, MO) to retarget the RNA portion of the intron. Primers were designed to introduce nucleotide substitutions into the IBS, EBS2, and EBS1d regions of the LtrBL1 intron originating from *Lactococcus lactis* using the InGex Intron Prediction Program accompanying the targetron products (www.Sigma-Aldrich.com/Targetronaccess). *S. aureus* intron-donor vector pNL9162 was used as a template for PCR reactions to construct *pyk*-specific targetron donor plasmids pPK312s, pPK357s, pPK390s, and pPK77a containing the *pyk*-specific IBS-EBS fragments (350 bp) between the *Hin*dIII and *Bsr*GI sites inserting LtrBLl targetrons into the selected sites in the *pyk* gene. *Pyk*-specific targetron donor plasmids were electroporated into *S. aureus* RN4220. Transformants were grown until early log phase when intron invasion was induced by 10 μM $CdCl_2$ at 37 °C. After overnight induction, cells were isolated on BHI plates containing 10 μg/mL erythromycin. The intron insertions were identified by colony PCR, using the genomic DNA from these mutants as templates and specific PK primers flanking the predicted insertion sites in the *pyk* gene. The amplified fragments were cloned into pUC19 (Sigma-Aldrich) and sequenced to confirm the intron insertion. Attempts to cure the *pyk* targetron plasmids by plate-streaking the insertion mutants on BHI (no erythromycin) at 37−40 °C to identify erythromycin-sensitive mutants failed. Due to the temperature sensitivity of the IEP-assisted splicing reaction in targetron system, wild-type cells, transformants having uninduced *pyk* donor plasmids, and *pyk* disruptants in sense orientation were streaked on plates incubated separately at 32 and 43 °C to access the essentiality of PK for growth. The plates were incubated for 24−48 h and photographed. Control

parent strain and induced transformants of pPK390s were grown in BHI medium overnight at 32 °C, then diluted 1:20 into fresh medium, and incubated for 4 h at 32 °C or for 2 h at 43 °C. RNA was extracted and analyzed by RT-PCR, using PK-specific primers flanking the *pyk*390s intron inserted in the *pyk* gene. Primers sequences are available upon request. Control RT-PCR experiments were performed when the initial reverse transcription step was omitted or the reactions were carried out in the absence of RNA substrate. Disruption of *hsa,* a previously confirmed essential gene in *S. aureus*, was performed as a control (*30*).

The 6-phosphofructokinase gene (*pfk*) was also disrupted independently by insertion of the group II intron at position 363 in the antisense strand of the gene.

Evaluation of PK Expression and Enzymatic Activity during the S. aureus Life Cycle. Turbidity growth curves were generated for *S. aureus* strain RN4220 in BHI at 37 °C by measuring cell density at OD_{600}. Cultures were inoculated with bacterial suspensions at an initial OD_{600} of 0.1, equal to the concentration of approximately 10^7 CFU/mL. Growth rates were determined for up to 24 h in three independent experiments performed in duplicate. PK expression and enzymatic activity were also determined at different time points of parallel cultures. Cells were harvested at various time points, washed with PBS, and then lysed for 30 min at 37 °C in lysis buffer (20 mM Tris-HCl, pH 7.5, 150 mM NaCl, 100 μg/mL lysozyme, 100 μg/mL lysostaphin, 0.04% Triton X-100, 16 μg/mL DNase I, 1.6 mM $MgCl_2$, 0.5% NP-40, 1 mM DTT, and Complete protease inhibitor). Cell debris was pelleted by centrifugation at 25000*g* for 20 min, and soluble cell extracts were further filtered through a 0.8 μm filter. MRSA cell extract (50 μg) was used to determine PK enzymatic activity at different phases of *S. aureus* growth as described above.

To assess PK protein expression, 2 μg of cell extracts obtained from different time points was subjected to 12% SDS−PAGE and transferred to polyvinylidene difluoride membranes (Millipore) for immunoblotting. The primary antibody was a rabbit polyclonal anti-MRSA PK generated in this study, and the secondary antibody was goat anti-rabbit horseradish peroxidase (BioSource International). The blots were developed using an ECL chemiluminescence kit (Amersham Biosciences) and exposed to X-ray film for 2−10 s, conditions under which each exposure to the film does not reach saturation. Resultant films were scanned and quantified using ImageJ software (NIH). The quantified protein bands were plotted using the intensity of the band in the peak fraction as 1 and quantifying the amount of the protein in surrounding fractions as a percentage of that in the peak lane. Blots were stained with Ponceau S after development to provide a control for equal loading of the MRSA lysate.

Generation of PK Constructs. Genomic DNA of MRSA strain Sanger 252 extracted using the Dneasy tissue kit (Qiagen) was used as a template to generate the His-tagged MRSA PK apoenzyme (Met^1−Leu^{585}) (MRSA PK_{WT}), as well as a His-tagged PK mutant truncated at the extra C-terminal domain (Met^1−Val^{472}) (MRSA PK_{CT}) by introduction of a stop codon at the appropriate loci. The boundary for generation of the C-terminal truncation was selected based on homology with other extra C-terminal-containing PKs (i.e., *B. strearothermophilus*). The following primer sets were used, creating appropriate restriction sites (*Nde*I and *Xho*I sites underlined) for cloning of MRSA PK_{WT} (M27F, 5′-CTACATATGAGAAAAACTAAA-ATTGTATG-3′, and M27R, 5′-GTTCTCGAGTTATAGTAC-GTTTGCATATCCTTC-3′) and MRSA PK_{CT} (M27F and M27CTR, 5′-GTTCTCGAGTTAAACTAGGTGGATTTTC-ATC-3′). The resulting PCR fragment for each construct was cloned into *Nde*I and *Xho*I sites of the bacterial expression vector pET-28a(+) (Novagen) providing an N-terminal 6× His tag to generate pET-28a-MRSA PK_{WT} and pET-28a-MRSA PK_{CT}. DNA of *E. coli* strain O157:H7 (Sakai) (courtesy of Dr. B. Finlay, University of British Columbia, Canada) was used as a template to generate the full-length *E. coli* PK1 (NP_310410) and PK2 (NP_310591) enzymes. The following primers were used for cloning using *Nde*I/*Bam*HI sites (underlined) for PK1, 5′-CTA-CATATGAAAAAGACCAAAATTGTTTGCACCATC-3′ and 5′-GTTGGATCCTTACAGGACGTGAACAGATGCGGTG-TTAG-3′, and *Nde*I/*Xho*I sites (underlined) for PK2, 5′-CTA-CATATGTCCAGAAGGCTTCGC-3′ and 5′-GTTCTC GAG-TTACTCTACCGTTAAAATACGCGTGG-3′. The resulting PCR fragments were cloned as indicated above into the corresponding sites of pET-28a(+) to generate pET-28a-PK1 and pET-28a-PK2 that generated N-terminally His-tagged recombinant *E. coli* PK isoforms. The sequence and the correct reading frame of all constructs were verified by sequencing.

Production of Anti-MRSA PK Antibody. Polyclonal PK antibody was produced by immunization of rabbit with purified recombinant His-tagged MRSA PK_{WT} according to standard protocols (Pacific Immunology Crop, Canada).

Expression and Purification of Recombinant His-Tagged MRSA and E. coli PKs. MRSA and *E. coli* constructs in pET-28a(+) vector were used to generate relevant recombinant PK proteins in *E. coli* BL-21(DE3). The proteins were expressed and purified using Ni-NTA agarose (Qiagen) according to the manufacturer's protocol. Briefly, cells were grown to an absorbance of 0.4−0.5 at 600 nm in 2 × YT medium and then induced with 0.1 mM IPTG for 3 h at 20 °C. Cells were lysed by sonication on ice (3 × 10 s bursts with a 30 s recovery between bursts) in lysis buffer (0.2 mg/mL lysozyme, 50 mM Tris, pH 7.5, 10 mM $MgCl_2$, 200 mM NaCl, 100 mM KCl, 10% glycerol, 10 mM imidazole, 0.5% NP-40, and 1 mM DTT containing Complete protease inhibitor). Cell lysates were cleared by centrifugation (20000 rpm in a Beckman JA-20 rotor) for 20 min at 4 °C, and PK isoforms were purified by batch binding to Ni-NTA resin. The resins were then packed in columns (1 × 2 cm) and washed with 400 column volumes of lysis buffer containing 30 mM imidazole. His-tagged PK isoforms were eluted with the same buffer containing 300 mM imidazole. The proteins were dialyzed overnight at 4 °C versus 2000 volumes of ice-cold 30 mM Tris, pH 7.5, 25 mM KCl, 5 mM $MgCl_2$, 10% glycerol, and 1 mM DTT to remove imidazole. All purification steps were done at 4 °C; enzymes were flash-frozen and stored at −70 °C where activity was found to be stable for at least 10 months. No loss of enzyme activity was observed with up to five freeze−thaw cycles. The purity and physical integrity of proteins were assessed using SDS−polyacrylamide gel electrophoresis (SDS−PAGE) followed by Coomassie Blue staining or immunoblotting. Protein concentration was estimated by Bradford assay (Bio-Rad protein assay) using bovine serum albumin as standard.

Quaternary Structure Determination. The molecular masses of the recombinant proteins were determined by size exclusion chromatography. Purified His-tagged full-length and extra C-terminally truncated MRSA PK (0.25 mg) in buffer B (30 mM Tris-HCl, 25 mM KCl, 3% glycerol, and 1 mM DTT) were injected independently onto a Superdex 200 HR (10 mm × 30 cm) column run on the AKTA Purifier liquid chromatography system (Amersham-Pharmacia Biotech) equilibrated with the

same buffer. The proteins were eluted at a flow rate of 0.7 mL/min at 4 °C. Elution positions were determined using the PK assay. For reference, 2.0 mg of a protein standard mixture (Bio-Rad) was applied to the same column and eluted using the same protocol. The molecular mass of each protein was determined from the standard curve based on elution volumes.

Measurement of Pyruvate Kinase Activity. PK activity was determined using a modification of published methods (*23*), by a continuous assay coupled to lactate dehydrogenase (LDH) in which the change in absorbance at 340 nm owing to oxidation of NADH was measured using a Benchmark Plus microplate spectrophotometer (Bio-Rad). The reaction contained 60 mM Na^+-HEPES, pH 7.5, 5% glycerol, 67 mM KCl, 6.7 mM $MgCl_2$, 0.24 mM NADH, and 5.5 units of L-LDH from rabbit muscle (Sigma-Aldrich) in a total volume of 200 μL. Two millimolar ADP and 0−30 mM PEP (for experiments to determine $S_{0.5}$ for PEP in the presence or absence of 1 mM AMP) or 0−5 mM ADP and 20 mM PEP (for experiments to detrmine $S_{0.5}$ for ADP) or 2 mM ADP and 10 mM PEP (for experiments to locate the elution position of proteins or assess specific activity of native enzyme in different phases of *S. aureus* growth) were added as substrates. Reactions were initiated by addition of one of the following PK enzymes: MRSA PK_{WT} (15 nM), *E. coli* PK isoforms (15 nM), MRSA PK_{CT} (200 nM), or MRSA cell lysate (50 μg). PK activity proportional to the rate of change at 340 nm was expressed as specific activity (μmol min^{-1} mg^{-1}), which is defined as the amount of PK that catalyzes the formation of 1 μmol of either product/min. The apparent $S_{0.5}$, Hill coefficient (h), and V_{max} or k_{cat} values were determined by allosteric sigmoidal nonlinear regression analysis of data using the Prism software package of Graph Pad Inc. (San Diego, CA). The molecular masses of the MRSA His-tagged wild-type (PK_{WT}), truncated (PK_{CT}), and the native PK enzyme as monomers are assumed to be 65168, 53639, and 63142 Da, respectively. In all studies, less than 10% of total PEP was exhausted during the reaction. Reactions were performed at 30 °C for 5 min. All values determined represent three measurements, each in triplicate.

Definition of Major Kinetic Parameters. Turnover number (k_{cat}) is the number of catalytic events per second per mole of active site. $S_{0.5}$ is the substrate concentration at which the reaction velocity is half-maximal. Hill coefficient (h) is an empirical parameter related to the degree of cooperativity; values larger than unity indicate positive cooperativity among ligand binding sites of different subunits.

Calculation of Free Energy of Binding. The value for the Gibbs free energy change, ΔG, that occurs by association of PEP or ADP with MRSA PK is related to the equilibrium association constant for the interaction and was calculated using eq 1:

$$\Delta G = -RT \ln K \quad (1)$$

where $K = K_m$, R is the ideal gas constant (equal to 1.98×10^{-3} kcal deg^{-1} mol^{-1}), and T is the temperature at which the assay was done (303 °K).

The contribution of CT domain to the Gibbs free energy of binding in an enzyme−transition state complex was calculated from eq 2:

$$\Delta\Delta G = \Delta G_{WT} - \Delta G_{CT} \quad (2)$$

$\Delta\Delta G$ is the change in free energy of binding in enzyme−transition state complexes attributable to the CT truncation.

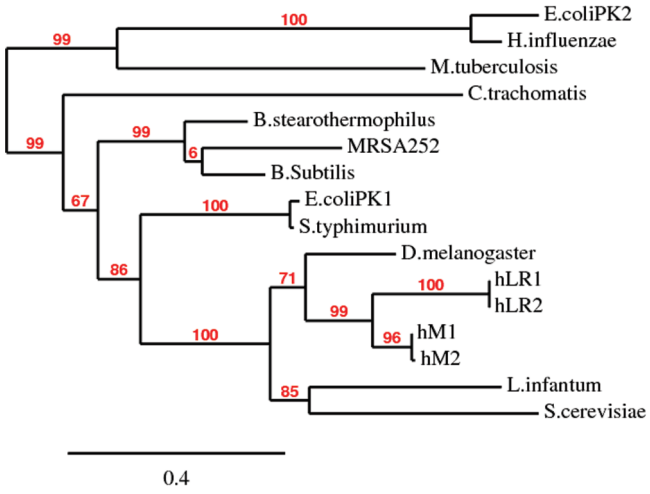

FIGURE 2: Phylogenetic (neighbor-joining) tree constructed using pyruvate kinase amino acid sequences. The accession numbers, in addition to those indicated in Figure 1, are as follows: *Saccaromyces cerevisiae* (NP_009362.1), *Bacillus subtilis* (NP_390796), *Haemophilus influenzae* (AAX88293), and *Leishmania infantum* (XP_001468820). Sequences were aligned using the ClustalW software (*36*). The phylogenetic tree was constructed using the phylML (*59*).

RESULTS

Bioinformatic Analysis of MRSA PK. Genome sequence analysis of a number of *S. aureus* strains for which such sequences are available (e.g., MRSA252: NC_002952.2) revealed that *pyk* in *S. aureus* exists as a single copy gene located 22 nucleotides downstream of 6-phosphofructose (PFK) gene (*pfk*) in a tandem *pfk*−*pyk* arrangement. This suggests that *pyk* and *pfk* genes form a bicistronic operon in *S. aureus*. No significant ORF was found in the 345 nucleotides downstream of the *pyk* gene, indicating that the tandem *pfk*−*pyk* arrangement was not associated with another gene. The operon association between *pyk* and *pfk* was previously observed in some other Gram-positive organisms such as *L. bulgaricus* (*31*, *32*), *L. lactis* (*33*), *Mycoplasma genitalium* (*34*), *B. stearothermophilus*, *Streptococcus bovis*, *Bacillus psychrophilus*, and *Bacillus licheniformis* (*35*). Although both of these enzymes are closely related in glycolysis, the biological significance of this operon remains unclear (*28*).

The amino acid sequence of the MRSA PK was compared to the sequences present in the GenBank/EMBL databases using BLAST (*36*). As expected, high homologies between bacterial PKs were found in the protein databases. The highest score was obtained for *Staphylococcus* sp. (85−100% identity). The next highest homologies were with *Bacillus* sp. (e.g., 62% identity with PK from *B. stearothermophilus*), *Enterococcus faecalis* (60% identity), *Listeria* sp. (58% identity), *E. coli* PK1 (48% identity), and *E. coli* PK2 (39% identity). The higher identity with the type I isoenzyme of *E. coli* (e.g., PK1) suggests that the MRSA PK belongs to the type I group. The phylogenetic relationships represented in Figure 2 showed a wide divergence between MRSA PK and human isozymes. Phylogenetic analysis also clearly revealed the significant evolutionary distance existing between the type I and type II (e.g., *E. coli* PK2) isoenzymes in Gram-negative bacteria. The distinction, however, is not so definite in Gram-positive microorganisms. PK from *B. stearothermophilus* (*16*), which is known to have all of the characteristics of a type II isoenzyme, is found clustered with the other Gram-positive enzymes. Thus, the appurtenance of the PK from a Gram-positive bacterium to one type of *E. coli* isoenzyme cannot be determined solely

on the basis of primary sequence homologies; biochemical properties must also be considered.

MRSA PK was found to have an extra C-terminal extension (CT) of 112 residues reported previously only in Gram-positive bacteria such as *Bacillus* sp. (*28*, *35*), *L. bulgaricus* (*31*), and *L. lactis* (*31*) (Figure 1). The MRSA CT domain composed of residues Gly^{473}−Leu^{585} (Figure 1) encodes a motif (PROSITE no. PS00742) characteristic of mobile PEP-utilizing enzymes such as pyruvate, orthophosphate dikinase (PPDK, EC 2.7.9.1) found in plants, PEP synthase (EC 2.7.9.2) essential for gluconeogenesis, or the PEP−protein phosphotransferase (EC 2.7.3.9), i.e., enzyme I (EI) of the PEP-dependent sugar phosphotransferase system (PTS). In these enzymes, the phosphoryl group transferred to PEP is transiently carried by a conserved histidine residue. Interestingly, this histidine residue was found to be replaced by a proline in *S. aureus* PK (e.g., P; residue 539 in MRSA252). The biological role of this domain in PKs has not yet been fully elucidated. However, it has been suggested that the CT extension may play a role in the structural stability of the enzyme through its interaction with the A domain at the subunit interface (*6*). The presence of this extra C-terminal domain suggested a possible dual function for the MRSA PK, where PEP can be transformed into pyruvate either by the classical PK activity that produces ATP or by the potential phosphotransferase activity that does not produce ATP but possibly phosphorylates another target that could be either a small metabolite or a protein [e.g., the phosphoryl carrier protein (HPr) of the PTS]. In the present study, we analyzed the actual impact of CT domain on MRSA PK structure and function by characterization of a C-terminally truncated PK mutant.

The sequence alignment of PKs from various eukaryotes and a wide variety of both Gram-positive and Gram-negative bacteria using ClustalW software (*36*) revealed sequence divergence and several amino acid insertions and deletions which clearly delineate eukaryotic PKs from those of bacterial origin (Figure 1). The homologies of the MRSA PK amino acid sequence to the corresponding sequences of human M1, M2, L, and R were 45%, 44%, 43%, and 43%, respectively, due to the highly conserved residues within PK. Multiple alignment of amino acid sequences of bacterial PKs with those of human enzymes (Figure 1) revealed that the known binding sites for ADP, PEP, and cations, located in the A and B domains, are well conserved (76−100%), whereas sites for effector binding, located in domain C, are not conserved. In addition, some deletions in the A domain and in the vicinity of the effector binding site in the C domain were found to be unique to bacterial PKs (Figure 1). These unique sites could be targets for the design of selective inhibitors. In this regard, homology modeling (Cherkasov et al., unpublished results) showed that the high level of sequence (Figure 1) and structural divergence between bacterial and mammalian PKs should permit the development of specific inhibitors for bacterial PK.

Essentiality Testing of S. aureus PK. As part of a genome-scale analysis of essentiality in *S. aureus* using inducible antisense RNA expression, Forsyth and colleagues (*37*) identified that PK is critical for growth. However, it was not clear whether expression of PK antisense RNA leads to lethal isogenic or growth-defective strains. Moreover, definitive determination of PK essentiality using antisense inhibition is particularly problematic due to the potential polarity effect of PK-specific antisense RNA on the expression of the upstream *pfk*. Recently, "targetron", a gene knockout system that utilizes the *L. lactis* Ll.LtrB group II intron, has been adapted for gene disruption in a growing number of bacteria including *S. aureus* (*38*). In order to formally prove the essential nature of this protein, the targetron system was used to knockout PK gene with an intron donor plasmid expressing LtrBLl and LtrA under the control of Pcad promoter with a temperature-sensitive replicon (*30*). Toward this end, *pyk* was disrupted independently at one target site in antisense orientation (*pyk*77a) and three different target sites in sense orientation (*pyk*312s, *pyk*357s, and *pyk*390s). More than 200 transformants were obtained from the electroporation of strain RN4220 with each *pyk* targetron donor plasmid that mediated intron integration into the site-specific *pyk* antisense and sense strands (e.g., pPK77a, pPK312s, pPK357s, and pPK390s, numbered from its translation start codon).

Cadmium induction was necessary to obtain *pyk* disruptants since Pcad promoter had a low basal level of transcription in the absence of cadmium. Ten colonies were PCR-screened from cells without cadmium induction for each *pyk* targetron, and none of them had the desired disruption. In contrast, after cadmium induction, 4, 6, and 9 of 10 colonies had the desired disruption for *pyk*312s, *pyk*357s, and *pyk*390s targetrons, respectively. Thus the total insertion frequency of the intron at nt 312|313s, 357|358s, and 390|391s of *pyk* was calculated to be (approximately) 40%, 60%, and 90%, respectively. Attempts failed to get any *pyk* disruptant with *pyk*77a despite screening up to 100 induced colonies. The inability to get *pyk* intron insertion in the antisense orientation may indicate the essentiality of the *pyk* gene, since in principle, targetron inserted in the antisense orientation is transcribed into the complement of the intron RNA sequence and cannot be spliced, yielding an unconditional *pyk* disruption. PK gene fragments were amplified from a subset of induced *pyk*390s targetrons (Figure 3A, lanes 1−7; 1.2 kb) versus the control parent cells (Figure 3A, WT; 0.28 kb) and uninduced pPK390 transformant (Figure 3A, T; 0.28 kb). The size and sequencing results (data not shown) of the amplified *pyk*-intron fragments verified the presence of the LtrBL1 intron integrated into the site-specific *pyk* sense strand (e.g., at the site between nt 390 and 391 of *pyk*). The smaller PCR product (Figure 3A, WT and T; 0.26 kb) was derived from *pyk* gene without the inserted intron, and the larger product (Figure 3A, lanes 1−7; 1.2 kb) is derived from the *pyk* gene containing the inserted intron.

LtrA protein could potentially remobilize or splice out the inserted intron if it was integrated in the sense orientation; therefore, it was desirable to cure the targetron plasmids from the disruptants prior to analysis. However, the donor plasmid could not be cured if the targeted gene was essential because the IEP-assisted splicing of the inserted intron was required to produce essential protein. Several attempts made to cure the *pyk* targetron plasmids (*pyk*312s, *pyk*357s, and *pyk*390s) were unsuccessful, indicating the essential nature of the *pyk* gene. Nevertheless, temperature sensitivity of the IEP-assisted splicing reaction in the targetron system made it possible to obtain conditional disruptants for introns integrated in the sense orientation by growth at elevated temperature (e.g., 43 °C). PK gene disruption by targetron yielded conditional *pyk* disruptants that grew at 32 °C (inserted intron spliced out) but not at 43 °C (inserted intron disrupted *pyk*) for *pyk*390s (Figure 3B), *pyk*312s, and *pyk*357s (data not shown). The *hsa*24s targetron was also used as a control to disrupt the previously shown essential hsa gene (Figure 3B). To confirm that the temperature sensitivity of the *pyk* disruptants was due to the temperature-sensitive IEP-assisted splicing reaction of the inserted intron, the splicing of the *pyk*390s intron inserted in the PK gene was assayed after the

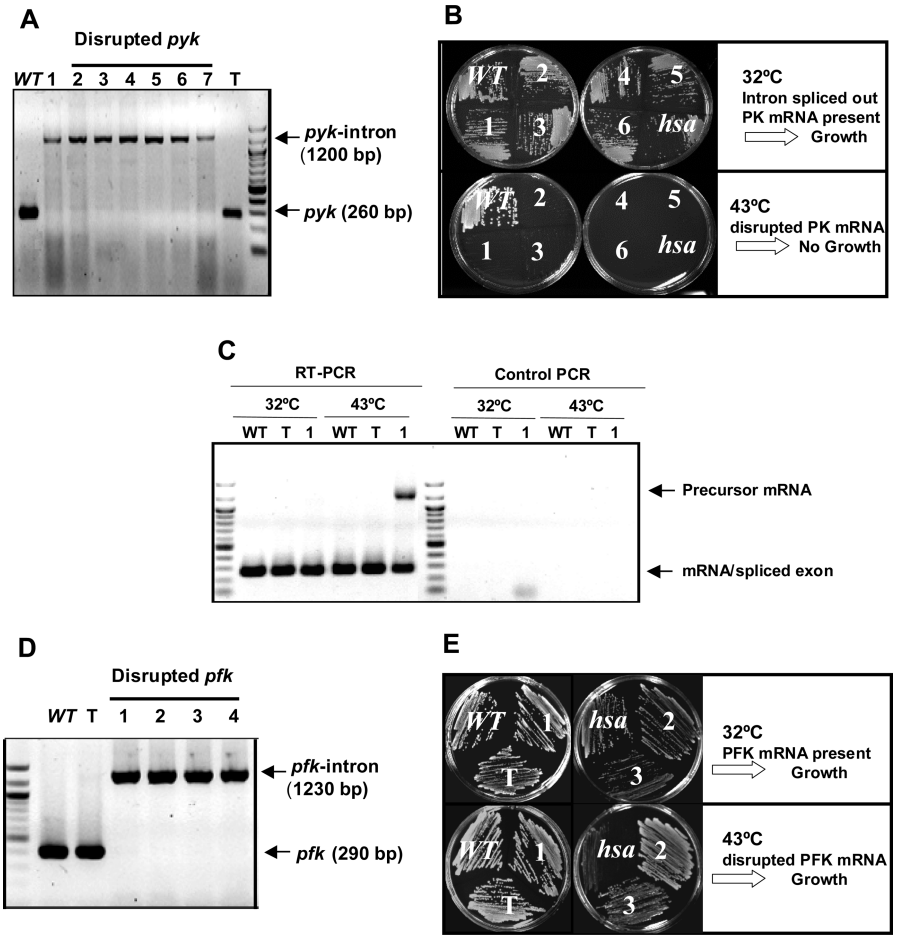

FIGURE 3: Disruption of the PK and PFK genes in *S. aureus* using targetron-mediated intron insertion. (A) Detection of *pyk*390S-intron integration. Colony PCR was performed on control parent strain (RN4220:WT) and *pyk* disruptants (1−7) and uninduced pPK390 transformant (T) utilizing specific PK primers for the DNA flanking intron insertion site (390|391s). Cells were grown at 32 °C. (B) Plating assay. Wild-type RN4220 (WT), induced *pyk* disruptants obtained with pPK390 (1−6), and hsa disruptant obtained from pNL9164 were streaked on BHI agar plates at 32 and 43 °C. The plates were incubated for 24−48 h and photographed. (C) RT-PCR assay of pyk390-intron splicing from the *pyk* gene. Control parent strain (RN4220:WT) and induced transformants of pPK390 (1−2) were grown in BHI medium overnight at 32 °C, then diluted 1:20 into fresh medium, and incubated for 4 h at 32 °C or for 2 h at 43 °C. RNA was extracted and analyzed by RT-PCR, using PK-specific primers flanking the *pyk*390 intron inserted in the *pyk* gene. Controls showed no products if the initial reverse transcription step was omitted, indicating that the amplified bands in the experimental samples are derived from cellular RNA. (D) Detection of *pfk*363A-intron integration. Colony PCR was performed on control parent strain (RN4220:WT) and *pfk* disruptants (1−4) and uninduced pPFK363 transformant (T) utilizing specific PFK primers for the DNA flanking intron insertion site (363|364a). Cells were grown at 32 °C. (E) Plating assay. Wild-type RN4220 (WT), cured uninduced pPFK363 transformant (T), cured induced *pfk* disruptants obtained with pPFK363 (1−3), and hsa disruptant obtained from pNL9164 were streaked on BHI agar plates at 32 and 43 °C. The plates were incubated for 24 h and photographed.

growth shift to 43 °C by RT-PCR using PK-specific primers flanking the intron-insertion site (Figure 3C). At 32 °C, in the wild-type (WT) strain and the uninduced transformant, the product was a 0.26 kb band corresponding to PK mRNA (Figure 3C, WT and T), and this same band, corresponding to mRNA with spliced exons, was also the product in the *pyk*390s disruptant (Figure 3C, 1). Strikingly, when cells were grown overnight at 32 °C and shifted to 43 °C for only a short time (e.g., 2 h), the wild-type strain showed a single band (0.28 kb) corresponding to *pyk* mRNA without the inserted intron as expected (Figure 3C, WT), while the *pyk* disruptant showed substantial accumulation of the larger band (1.2 kb) derived from the precursor RNA containing the inserted intron, with concomitant reduction in the intensity of the band corresponding to the mRNA with spliced exons (Figure 3C, 1).

In summary, results of *pyk* targetron inactivation at four independent different target sites in both sense and antisense strands indicated that the PK gene is an absolutely essential gene for *S. aureus* viability. On the other hand, PFK was identified as a nonessential gene in *S. aureus*, as a nonconditional knockdown strain that was generated using confirmed intron insertion to the *pfk* at position 363 of the antisense strand grew even after curing the donor plasmid at both 32 and 43 °C (Figure 3D,E). These results confirm the suggestion that PK is essential in *S. aureus* but contradict the results of a previous work demonstrating PFK essentiality using an antisense strategy (*37*).

PK Expression and Enzymatic Activity Increases during Exponential Phase of S. aureus Growth. It was previously shown that almost complete depletion of glucose occurs during the exponential phase of *S. aureus* growth (*39*). We expected that glucose depletion would correlate with increased PK expression and/or activity in the exponential phase of growth so that inactivation of essential PK protein could lead to growth inhibition by limiting the ability of *S. aureus* to catabolize glucose. In order to test this hypothesis and characterize the role of the PK in the *S. aureus* life cycle, PK expression and specific enzymatic activity was analyzed during growth of *S. aureus* in liquid culture (Figure 4). Expression of PK protein was found to be increased

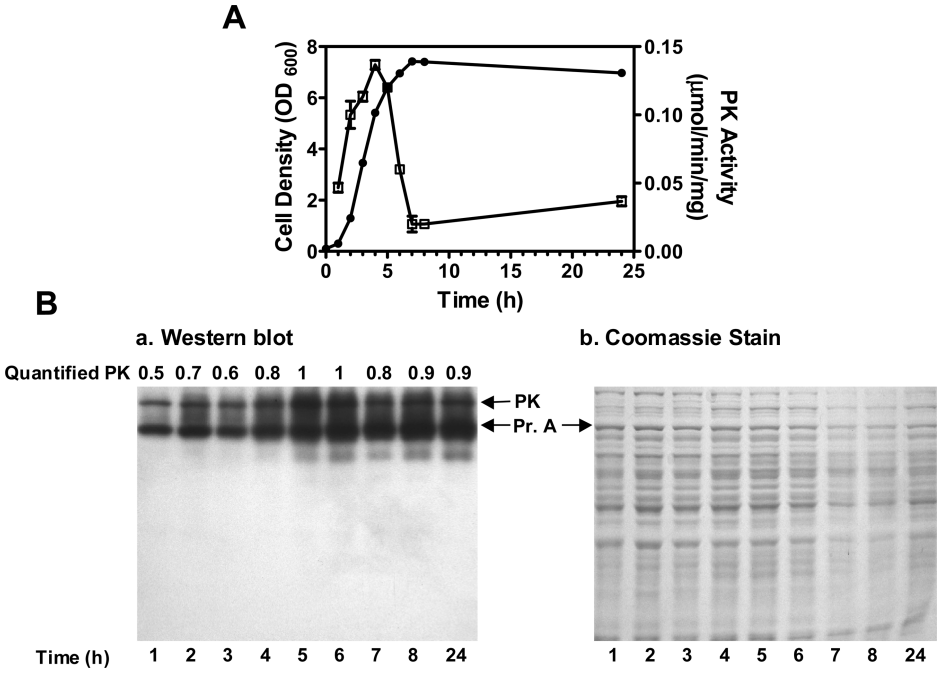

FIGURE 4: PK expression and enzymatic activity profile during *S. aureus* life cycle. Two independent *S. aureus* cultures were grown in parallel in BHI after inoculation with an initial cell density of $OD_{600} = 0.1$. (A) At indicated time points, an aliquot was removed, appropriate dilutions were made, and the cell density (●) was determined at OD_{600}. Aliquots were also removed at the exponential, postexponential, and stationary phases of growth (1−5, 7−8, and 24 h, respectively), and specific PK activity was determined (□) as described in Materials and Methods. (B) Expression of PK was detected using anti-PK polyclonal antibody and quantified as described in Materials and Methods. The same gel was stained with Coomassie Blue to show equal protein loading (right panel). The results presented are representative of three independent experiments.

(by 50%) during the exponential phase of growth (e.g., 1−4 h), reaching maximal levels as bacteria entered the postexponential phase of growth (e.g., 5−6 h) (Figure 4B). PK enzymatic activity was also found to rapidly increase (by 2.8-fold) during the exponential growth phase (e.g., 1−4 h), and this correlated with expression of PK protein up until approximately 5 h. In contrast, during the postexponential phase of growth, there was a sharp drop in PK enzymatic activity while the PK protein levels remain relatively constant, indicating posttranscriptional regulation of PK activity in the stationary phase of growth. In addition, the minimal PK activity in the stationary phase might be a result of less substrate (PEP) availability due to the reduced pool of glucose. These data show that PK expression and enzymatic activity clearly correlate with the phase of bacterial growth and are highly regulated during the bacterial life cycle (Figure 4A). The important role of PK in *S. aureus* growth is in agreement with the results of previous work demonstrating a substantial reduction of growth rate (by 70%) in a PK mutant of *B. subtilis* (*40*).

Expression and Purification of PK Proteins. Functional features of the MRSA PK were defined by creating and characterizing the biophysical and biochemical properties of recombinant His-tagged proteins including wild-type MRSA PK containing the full-length sequence, PK_{WT} (Met^1−Leu^{585}), as well as a PK mutant truncated at the extra C-terminal domain PK_{CT} (Met^1−Val^{472}). Wild-type *E. coli* PK1 and PK2 isoforms were used as controls for determination of enzymatic characteristics of MRSA PKs. All proteins were expressed at high levels (∼30−40 mg/L of culture) using the bacterial expression system. Following purification as described in Materials and Methods, each exhibited a high degree of purity (>98%) as determined by SDS−PAGE [12% (w/v) gel] followed by Coomassie Brilliant Blue staining (Figure 5) or Western blot analysis for MRSA PKs using a polyclonal MRSA PK-specific antibody (results not shown). The estimated molecular mass of each of the respective bands on SDS−PAGE correlated well with that predicted based on the amino acid composition for each PK protein (Figure 5), indicating that all PK constructs were expressed as expected full-length proteins. MRSA PK proteins were further characterized with respect to their quaternary structure, kinetics of catalytic activity, and allosteric properties.

Assessment of the Oligomeric State of the PK Constructs. The molecular mass of wild-type PK was estimated by gel filteration on a Superdex 200 HR column. The gel filtration elution position of the MRSA PK was between those of the standard proteins: thyroglobulin (MW = 670 kDa) and bovine γ-globulin (MW = 158 kDa). The calculated molecular mass of the wild-type MRSA PK appeared to be 250 kDa (Figure 5B). This value was approximately quadruple that of the predicted molecular mass of a monomer of this construct (65.1 kDa) based on amino acid composition, suggesting that MRSA PK is tetrameric. The eluted fractions corresponding to the tetrameric form of PK were enzymatically active. Hence, like almost all pyruvate kinases from other organisms, active MRSA PK exists as a homotetramer. To investigate the impact of the CT domain on the quaternary structure of the enzyme, PK_{CT}, lacking the CT domain, was also analyzed. Based on its elution position, the calculated molecular mass was shown to be 215 kDa (Figure 5B) for PK_{CT}, consistent with a tetrameric structure compared with that predicted from the amino acid composition (53.1 kDa). Compared with wild-type PK, PK_{CT} migrated as a somewhat broader peak on gel filtration chromatography. This suggested that the extra C-terminal domain of PK may contribute to stabilizing the holoenzyme quaternary structure. The protein concentration of the peak fractions for wild-type PK following the Superdex 200 HR chromatography was determined by the Bradford method to be 250 nM, indicating that the K_D for

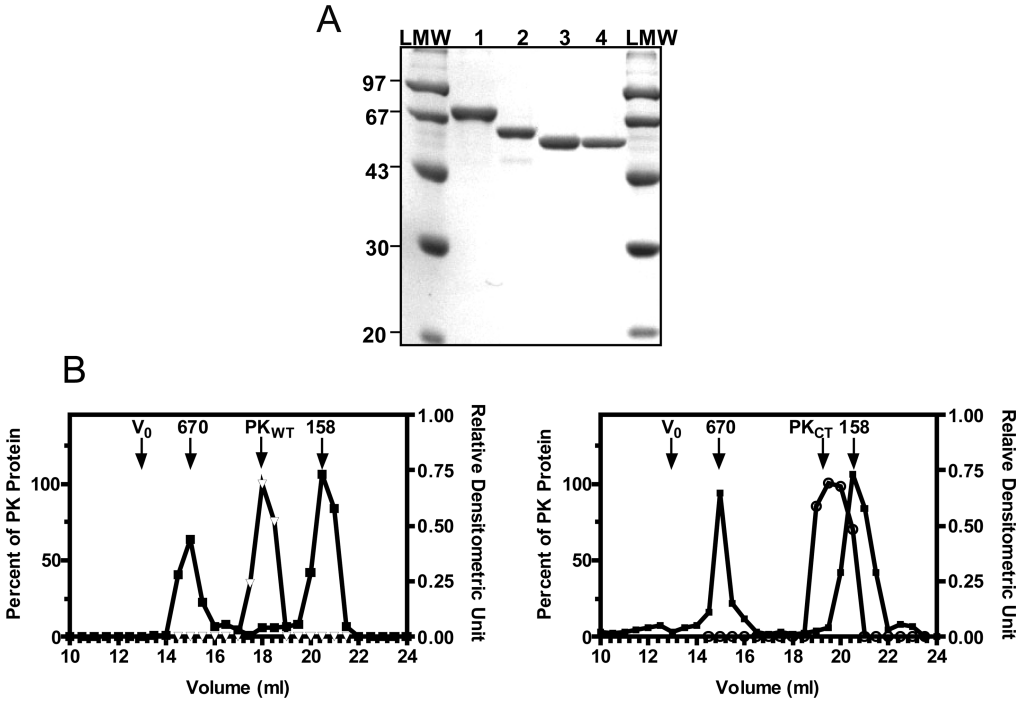

FIGURE 5: SDS−PAGE and size exclusion chromatography of recombinant wild-type and truncated MRSA PKs. (A) 5 μg aliquots of wild-type (PK_{WT}), C-terminally truncated mutant (PK_{CT}), and *E. coli* PK1 and PK2 proteins purified to homogeneity through the Ni-NTA chromatography step as described in Materials and Methods were applied to lanes 1−4, respectively. Low molecular weight (LMW) standards (Pharmacia Biotech) were applied as size markers. Proteins were visualized by staining the gel with Coomassie Brilliant Blue dye. (B) Wild type [PK_{WT} (▽), left panel] and C-terminally truncated mutant [PK_{CT} (○), right panel] were chromatographed separately on a 10/30 column of Superdex 200 HR, and positions of the proteins emerging in the effluent were monitored by PK activity as described in Materials and Methods. The molecular mass of each protein was determined from the standard curve generated from experiments with a protein standard mixture (Bio-Rad) applied to the same column and eluted using the same protocol. Elution positions of bovine thyroglobulin (670 kDa) and bovine γ-globulin (158 kDa) are indicated as separate curves (■). Results in these figures are representative of three experiments.

formation of a stable tetramer in MRSA PK is <250 nM. This finding indicated that tetramerization of the PK enzyme is not mediated by the CT domain. However, it does not rule out the contribution of the CT domain to tetramer stability.

Kinetic Properties of the Recombinant Wild-Type and Mutant MRSA PK. The specific activity (100 units/mg at 30 °C) of purified MRSA PK is comparable to values reported for other bacteria (*13*, *18*−*20*, *41*). To characterize the catalytic function of purified MRSA PK and to examine the impact of potential interactions of the CT domain on enzyme catalytic function and affinity for substrate, steady-state kinetics of recombinant (PK_{WT}) and truncated (PK_{CT}) MRSA PK were determined with respect to PEP in the absence and presence of 1 mM AMP and with respect to ADP as described in Materials and Methods (Figure 6). Parameters derived from these kinetics are summarized in Table 1. In the absence of the activator (AMP), both wild-type and truncated enzymes exhibited sigmoidal saturation curves for PEP, with comparable cooperation as expressed by Hill coefficients (h) of 2.8 (±0.4) and 2.3 (±0.5), respectively (Figure 6A,B), suggesting homotropic allosteric activation of enzyme by its substrate. These data indicate that the removal of the CT domain has minimal effect on the substrate cooperative interactions of enzyme. However, truncation of the CT domain produced a significant decline in the PK_{CT} catalytic activity (with k_{cat} value less than 6.8% of that for PK_{WT}) and a modest decline in affinity for PEP (with $S_{0.5}$ value of 1.6-fold that for PK_{WT}) (Figure 6A,B and Table 1). These results were verified using four separate preparations of purified PK_{CT} and show for the first time the importance of the CT domain for efficient PK catalysis.

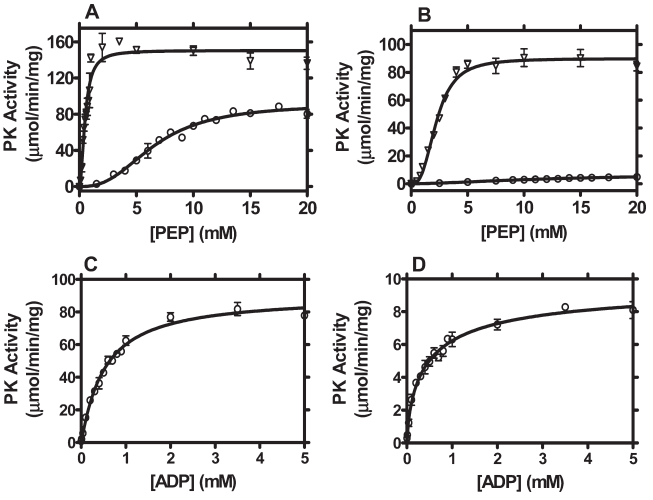

FIGURE 6: Steady-state kinetics of wild-type and extra C-terminally truncated MRSA PK. Steady-state kinetics of recombinant wild-type (A) and truncated (B) PK in the absence (○) or presence (▽) of 1 mM AMP as a function of PEP. Kinetics of wild-type (C) and truncated (D) MRSA PKs against ADP at fixed concentration of PEP (20 mM). PK assays were conducted as described in Materials and Methods. The data are derived from one of three experiments performed in triplicate and analyzed using Prism Graphpad software (single site model). Error bars indicate range of values within the single experiment shown.

The presence of activator (AMP) shifted the dependence of the wild-type initial velocity on the PEP concentration to a hyperbolic saturation curve, lowering h to 1.6 (±0.1), indicating decreased cooperativity (Figure 6A) as has been described for

Table 1: Kinetic Parameters of Recombinant MRSA PKs with Respect to PEP (in the Absence and Presence of 1 mM AMP) and ADP[a]

	PEP										ADP				
	AMP(−)					AMP(+)									
	V_{max} (μM min^{-1} mg^{-1})	k_{cat} (s^{-1})	$S_{0.5}$ (mM)	h	$k_{cat}/S_{0.5}$ ($\times 10^3$) (M^{-1} s^{-1})	V_{max} (μM min^{-1} mg^{-1})	k_{cat} (s^{-1})	$S_{0.5}$ (mM)	h	$k_{cat}/S_{0.5}$ ($\times 10^3$) (M^{-1} s^{-1})	V_{max} (μM min^{-1} mg^{-1})	k_{cat} (s^{-1})	$S_{0.5}$ (mM)	h	$k_{cat}/S_{0.5}$ ($\times 10^3$) (M^{-1} s^{-1})
PK_{WT}	90 ± 14	97.6 ± 14.8	6.6 ± 1.0	2.8 ± 0.4	59	167 ± 3	181 ± 3	0.6 ± 0.0	1.6 ± 0.1	1225	125 ± 19	136 ± 20	0.4 ± 0.1	1.1 ± 0.1	1360
PK_{CT}	8 ± 2	6.7 ± 1.3	10.5 ± 1.3	2.3 ± 0.5	2.5	87 ± 3	78 ± 3	2.1 ± 0.1	2.9 ± 0.3	146	9.6 ± 0.9	6.8 ± 0.8	0.4 ± 0.1	0.8 ± 0.1	85.7

[a] All values are the mean ± SEM of three experiments of triplicate determinations.

PK from other sources (*7*, *32*, *36*). The presence of AMP led to 11-fold decrease in the $S_{0.5}$ of PEP under nonsaturation conditions. Similarly, the presence of activator in the kinetics toward PEP shifted the sigmoidal curve of PK_{CT} to a hyperbole, while it had no effect on enzyme cooperativity (i.e., h = 2.9 ± 0.3) (Figure 6B). Inspection of the data in Table 1 shows that the apparent $S_{0.5}$ (PEP) values of truncated protein (PK_{CT}) were increased with respect to those of wild-type protein both in the absence (1.6-fold) and in the presence (3.6-fold) of 1 mM AMP.

Both proteins exhibited increased catalytic activity (k_{cat}) upon addition of AMP (Figure 6A,B and Table 1). However, the fold increase for truncated PK was significantly higher than that of the wild-type PK (k_{cat} values for wild-type and truncated PKs were 180.8 and 78.2 s^{-1}, respectively). This significant increase indicated that allosteric stimulation could restore the negative influence of the extra C-terminal domain truncation on the basal PK catalytic activity.

Steady-state kinetics of the wild-type PK and PK_{CT} as a function of ADP are shown in Figure 6C,D. Parameters derived from these kinetics are summarized in Table 1. Both proteins exhibited hyperbolic response to ADP with essentially identical $S_{0.5}$ values (0.4 ± 0.10) and comparable Hill coefficients (i.e., 1.1 and 0.8 for PK_{WT} and PK_{CT}, respectively) indicating no enzyme cooperativity. However, PK_{CT} had markedly reduced k_{cat} value (less than 4.9% that for PK_{WT}), indicating that removal of the CT domain also produced a particularly significant decline in the PK catalytic activity toward ADP. The fact that the catalytic activities of PK_{CT} toward both PEP and ADP were profoundly decreased compared to those of wild-type PK indicated that the CT domain may contribute to stability of the tetramer.

The energy involved in interactions of PEP and ADP with PK_{WT} were quantified from the K_m values for the respective substrate by calculating the Gibbs free energy of binding (ΔG) of 3.0 and 4.7 kcal mol^{-1}, respectively, as described in Materials and Methods. These values reflected the affinities with which the respective ligands bind to the PK catalytic site. The magnitude of the contribution of the CT domain to the binding energy in enzyme−transition state complexes ($\Delta\Delta G$) was quantified by calculating the Gibbs free energy of binding (ΔG) of PEP and ADP in PK_{CT} compared to the free energy of binding of these ligands in PK_{WT}. The change in the free energy of binding ($\Delta\Delta G$) of PK_{CT} for PEP and ADP was equivalent to 0.28 and 0 kcal mol^{-1}, respectively, indicating that the free energy of binding in the PK_{CT} with PEP was slightly reduced when compared to that of PK_{WT}. The fact that the truncated mutant bound ADP with essentially the same affinity as that of the wild-type PK indicated that overall structures of the truncated protein were preserved and that differences in its kinetic parameters were not due to nonspecific conformational effects induced by truncation. These data, on the whole, showed that there are no significant differences in the substrate affinity and allosteric regulation behavior between wild-type enzyme and truncated mutant. The findings suggest that the CT domain truncation only minimally perturbed the substrate and effector binding sites. However, the profoundly decreased catalytic activity of the CT domain-deleted mutant suggested the essential role of this domain in activity and perhaps stability of the MRSA PK in the active conformation.

Interestingly, neither wild-type nor CT truncated MRSA PK proteins responded significantly to either FBP (1 mM) or glucose 6-phosphate (1 mM) over a wide range of PEP and ADP concentrations, under both saturating and nonsaturating conditions (data not shown).

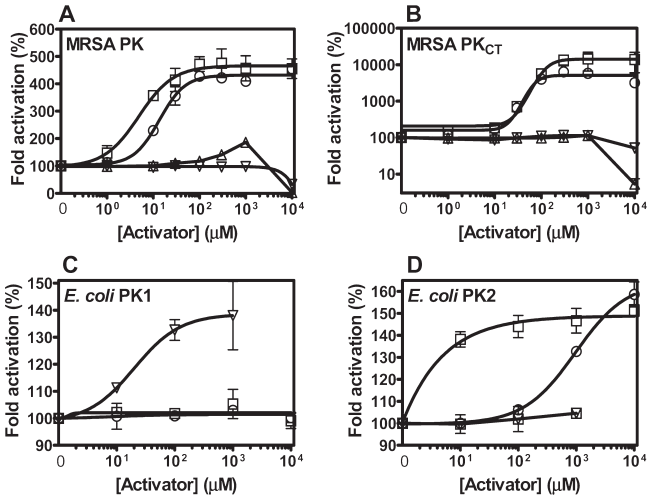

FIGURE 7: The allosteric regulation of MRSA PK. Kinetic response of recombinant wild-type (A) and truncated (B) MRSA PK as compared to that of *E. coli* PK1 (C) and *E. coli* PK2 (D) to AMP (○), R5-P (□), FBP (▽), and ATP (△). Enzymatic activity was assayed as described in Materials and Methods. The ADP and PEP concentrations were fixed at 2 and 5 mM, respectively. Percent of activity is based on the rate obtained in the absence of compounds.

Allosteric Regulation Profile of MRSA PK. To map the allosteric regulation profile of MRSA PK, specific activities of wild-type and truncated MRSA PK (Figure 7A,B) were determined at varying concentrations of FBP, AMP, ribose 5-phosphate (R5P), ATP, citrate, oxalate, and inorganic phosphate (P_i). Values of effects are reported in Table 2. The activation profile of each PK by effectors was presented as fold activation compared to that of the control (no compound) (Figure 7). Wild-type MRSA PK was activated by AMP and R5P with half-maximal concentrations (EC_{50}) of 14 and 5 μM, respectively. PK_{CT} was also activated by AMP and R5P but at greater magnitude compared to that of wild type. AMP and R5P at 1 mM showed 58- and 143-fold stimulatory effects on PK_{CT}, respectively, while they activated wild type by 4.1- and 4.6-fold, respectively, at conditions tested (Table 2). Nevertheless, a higher concentration of activator was needed for PK_{CT} activation (EC_{50} values for AMP and R5P were 4.8- and 24-fold larger than that of the wild-type enzyme, respectively). This significant difference in magnitude of activation might be explained by different affinities ($S_{0.5}$) for substrate between the two PK proteins, so that the PEP concentration used in the assay (5 mM) was saturating for wild type while is subsaturating for PK_{CT}. Furthermore, the results indicate that activation of truncated PK by both AMP and R5P was associated with increased cooperativity compared to that of wild-type enzyme (Table 2). These data demonstrate a possible regulatory role for the CT domain on allosteric activation of MRSA PK. Both wild-type and truncated PK enzymes were not activated by FBP, a known activator of PK enzymes (i.e., *E. coli* PK1 and human M2). In fact, FBP had an inhibitory effect (50−70%) on both proteins at 10 mM (Figure 7A,B). *E. coli* PK1 activation by FBP and *E. coli* PK2 activation by AMP and R5P were also determined as controls (Figure 7C,D). These results suggest that PK_{CT} exhibited a comparable activation profile to that of wild-type enzyme, indicating that the MRSA PK extra C-terminal domain is not essential for the allosteric nature of the enzyme but might regulate the magnitude of allosteric activation.

The effects of four potential inhibitors (oxalate, citrate, ATP, and P_i) on PK activity were also evaluated. Oxalate (an analogue of the enolpyruvate moiety of PEP and pyruvate) activated both wild-type PK and PK_{CT} at 1 mM. At higher concentration (e.g., 10 mM), the stimulatory effect of oxalate was preserved for PK_{CT}, while it was inhibitory for wild-type enzyme (60%) (Table 2). Citrate inhibited enzyme activity of both PK proteins by 90% at 10 mM.

Table 2: Effectors of the MRSA PK[a]

activator	physiologic concn[b] (mM)	fold activation: activator at 1 mM	fold activation: activator at 10 mM	EC_{50} (mM)	h
MRSA PK					
AMP	0.28	4.1	4.5	0.014	1.6
ATP	1.5	1.9	0.0	ND[e]	ND
R5P	1.3[c]	4.6	4.6	0.005	1.2
FBP	15	1.0	0.3	ND	ND
citrate	2	0.8	0.0	2.7	1.4
oxalate	ND	1.7	0.4	ND	ND
P_i[d]	ND	0.3	0.0	0.37	1.2
MRSA PK_{CT}					
AMP	0.28	58	32	0.065	3.3
ATP	1.5	1.1	0.05	ND	ND
R5P	1.3[c]	143	139	0.12	2.9
FBP	15	1.1	0.5	ND	ND
citrate	2	0.9	0.1	1.3	ND
oxalate	ND	3.4	3.0	ND	ND
P_i[d]	ND	0.2	0.1	0.33	1.2

[a]Relative activities are presented. All values are the mean of three experiments of triplicate determinations. [b]According to refs *42* and *43*. [c]Concentration of pentose phosphates denotes the combined pools of R5P, ribulose 5-phosphate, and xylose 5-phosphate. [d]Inorganic phosphate. [e]ND: cannot be determined.

Interestingly, ATP exhibited a biphasic regulatory effect on MRSA PK activity in the presence of excess of Mg^{2+} (6.7 mM). Wild-type PK was activated by 2-fold at the physiologic range of ATP (e.g., 1 mM), while it was completely inhibited at ≥2.5 mM ATP in a noncompetitive manner. The biphasic regulatory effect of ATP on PK activity was lost in PK_{CT}, suggesting involvement of this domain in the regulation of enzyme activity by ATP (Figure 7B). The presence of succinyl-CoA was not required for ATP inhibition of MRSA PK, whereas it was shown in *E. coli* that ATP inhibition was dependent on succinyl-CoA (*56*). Inorganic phosphate (P_i) (K_2HPO_4−KH_2PO_4, pH 7.4) was a very effective inhibitor of both PK proteins, causing 70% inhibition at 0.2 mM concentration (data not shown). Wild-type PK was completely inactivated at 2.5 mM P_i. Thus PK_{CT} exhibited an activation profile comparable to that of wild-type enzyme, indicating that the MRSA PK extra C-terminal domain is not essential for the allosteric nature of the enzyme. However, it might influence the magnitude of allosteric activation.

In exponentially growing bacteria, ATP is present at a concentration of about 1.5−4 mM (*42*), whereas AMP and FBP concentrations are 0.28 and 15 mM (*43*), respectively, and the concentration of combined pools of pentose 5-phosphates are 1.3 mM. Results of the present study suggest that FBP and ATP inhibition combined with AMP and R5P activation may play a central role in regulating PK activity in MRSA.

DISCUSSION

The present study, for the first time, suggests that phosphofructokinase (*pfk*) and pyruvate kinase (*pyk*) constitute an operon in *S. aureus*, as a survey of available genome data for a

number of *S. aurues* strains revealed a tandem *pfk*−*pyk* arrangement. Independent expression of either PK or PFK antisense RNAs was sufficient to induce a lethal phenotype in *S. aureus* RN4420 strain (data not shown). In contrast, only PK was identified as an essential gene through independent chromosomal gene knockout experiments using targetron technology (Figure 3). These results establish the presence of a bicistronic operon for *pyk* and *pfk* in *S. aureus*. A *pfk*−*pyk* operon was previously found in some Gram-positive bacteria such as *S. bovis*, *L. bulgaricus*, *L. lactis*, *M. genitalium*, *B. stearothermophilus*, *B. psychrophilus*, and *B. licheniformis* (*28*, *31*−*35*, *44*). It appears that the *pfk*−*pyk* operon may be is a Gram-positive specific feature since no such operon association was reported in Gram-negative bacteria. However, the biological significance of this operon is not fully understood. Recent data suggest its involvement in transcriptional regulation of carbon catabolism in Gram-positive organisms (*45*).

We also provide direct evidence that *S. aureus* PK carries out a function that is absolutely essential for growth and viability of this key Gram-positive pathogen. This is based upon the finding that inactivation of chromosomal *pyk* by insertion of the group II intron at various positions of sense and antisense strands of *pyk* created a lethal phenotype. PK has been previously identified as a critical staphylococcal gene using conditional genome wide phenotypes generated by antisense RNA (*37*). However, it was not clear whether expression of PK antisense RNA resulted in lethal isogenic or growth-defective strains. Moreover, it was difficult from these studies to ensure gene-specific effects using antisense technology for genes configured in polycistronic operons where there may be polar effects. PK has been recently identified as an absolutely essential gene for survival of other bacteria such as *H. influenzae*, *Streptococcus pneumoniae*, and *Mycobacterium tuberculosis* using allelic replacement mutagenesis (*46*−*49*). The proven essential nature of PK in these bacteria is a very important feature of this enzyme, since products of genes that are essential for viability of the microorganism *in vitro* can be considered as potential drug targets in the effort to develop new classes of antimicrobial agents (*50*).

Our results clearly demonstrate that PK enzymatic activity is increased during growth of *S. aureus*, indicating the importance of PK for bacterial growth. Increased PK activity correlated with increased protein expression in the early phase of growth. However, enzyme activity dropped precipitously in the post-exponential phase while PK protein expression was maintained. Hence, it appears that PK activity is mainly modulated by tight allosteric regulation, as changes in the metabolic status of the bacteria in different phases of life cycle, particularly in the stationary phase, result in the attenuation of PK activity regardless of its abundance. PK activity has previously been shown to be important for growth of both Gram-negative (e.g., *E. coli*) and Gram-positive (e.g., *B. subtilis*) bacteria as PK mutant strains have substantial decreased growth rate (*39*, *51*).

In the present study, we report for the first time a detailed characterization of the biophysical and biochemical properties of an active recombinant *S. aureus* (i.e., MRSA) PK protein. Almost all known PKs characterized to date exist as tetramers of four identical subunits, each of which is comprised of four domains: N-terminal, A, B, and C domains. Our results indicate that the active recombinant PK of *S. aureus* also exists as a homotetramer. Characterization of tetramerization interactions have been reported for a number of PKs from seven species (e.g., *L. mexicana*, *E. coli*, *B. stearothermophilus*, *S. cerevisiae*, human, cat, and rabbit) (*52*). Tetramerization occurs through interactions between A and C domains of adjacent subunits so that bordering A domains constitute the A−A or "large" interface and adjacent C domains form the C−C or "small" interface between monomers. The amino acid sequences of A and B domains, containing the predicted substrate binding sites and cation binding sites, are well conserved in both prokaryotes and eukaryotes. However, the C-domain is variable in some organisms.

Our results confirmed that the predicted substrate (ADP and PEP) binding sites and cation binding sites located in A and B domains of bacterial PKs (e.g, MRSA PK) are well conserved when compared with those of human isozymes (Figure 1). In contrast, the predicted effector binding sites located in the C domain, which are involved in allosteric regulation of PK enzymes, are not conserved between bacteria and human isoforms. Some unique sequences, including a deletion, were identified in the predicted effector binding sites of the MRSA PK C domain (Figure 1). This is of particular interest for the design of selective inhibitors that act specifically against bacterial PK since selective targeting of human M2 PK containing a unique region for allosteric regulation recently provided an opportunity to target cell metabolism for cancer therapy despite the high amino acid homology (95%) and identical catalytic site of the M1 splice variant (*24*). This provides proof of principle that PKs may be selectively targeted despite high degrees of homology.

Our findings showed that both AMP and R5P (Figure 7) were heterotropic activators of PK and R5P was slightly more potent than AMP. We also found that MRSA PK exhibited homotropic positive cooperativity for PEP but not for ADP (data not shown). These findings suggest that the structure of the allosteric effector-binding site of MRSA PK differs from those of other PKs activated by FBP. A comparison of the predicted binding sites of the 6-phosphate moiety of FBP, located in the C-domain of MRSA PK, with the corresponding regions of other PKs is shown in Figure 1. In PKs activated by FBP, a conserved lysine (i.e., K; residue 433 in human M2) is thought to be involved in binding the 6-phosphate moiety of FBP (*11*). However, similar to nonallosteric enzymes (e.g., human M1 isozyme), MRSA PK has a glutamate at this position (i.e., E; residue 380) (Figure 1). This predicts that FBP should not be an allosteric activator of MRSA PK, and this is what we found (Figure 7A, Table 2). Hence, the observed properties of MRSA PK are consistent with the amino acid sequence data. The fact that MRSA PK was activated by AMP and R5P and not activated by FBP would appear to align MRSA PK with the type II group of bacterial PKs (e.g., *E. coli* PK2). However, this classification is contradicted by the higher identities at the amino acid sequence level with the type I group of bacterial PKs (e.g., 48% *E. coli* PK1).

Despite similarities in allosteric behavior to type II PKs, MRSA PK showed several interesting distinguishing properties. One feature of MRSA PK is that the enzymatic activity was inhibited at physiologic concentrations of FBP (Figure 6A). FBP is well-known to be an allosteric activator of most PKs including *E. coli* PK1 and several human PKs. To our knowledge a negative effect of FBP on any bacterial PK has been reported. Further investigations are necessary to clarify the physiological significance of the inhibitory effect of FBP on MRSA PK.

MRSA PK is the only bacterial PK characterized to date to show a dual response to ATP, as its activity was stimulated by low concentrations of ATP (e.g., 1 mM), but was completely

inhibited at higher concentrations of ATP (> 2.5 mM) (Figure 7A, Table 2). ATP has previously been shown to regulate PKs via a product feedback inhibition mechanism. On the other hand, ATP is known to be capable of chelating magnesium ions, which are necessary for PK enzymatic activity. Hence, the dual effects of ATP on MRSA PK are complex and difficult to analyze unambiguously. Although succinyl-CoA was shown to be necessary for ATP inhibition in *E. coli* (*21*), it is noteworthy that inhibition of the MRSA enzyme by ATP did not require the presence of succinyl-CoA (Figure 7, Table 2).

Based on our findings, a model of MRSA PK regulation might look something like this: during exponential growth of bacteria, ATP is rapidly depleted, and due to the shift of the V_{max} in the presence of the activator AMP (280 μM) and R5P (*43*), PK becomes highly active at the prevalent low PEP concentrations. By the time cells reach the stationary growth phase, the lack of readily available sugars has induced a reduction in the pentose phosphate pathway activity leading to depletion in the level of intracellular R5P. With the decreased energy requirement associated with the slowdown of cell metabolism, the level of ATP increases, which induces inhibition of the PK activity. This in turn induces an increase in PEP concentration, thus providing for a continued source of energy in the context of residual PK activity leading to the production of ATP. Should a carbohydrate substrate become once more available to the cell, owing to the high potential of R5P as an activator, PK is able to resume a high level of activity, thereby providing ATP for glycolysis and the restoration of normal cell functions. Thus, PK plays a key role in the modulation of glycolysis and cell metabolism in bacteria.

A remarkable characteristic of staphylococcal PKs (e.g., MRSA PK) and a few other bacteria (e.g., *Bacillus* sp., *Listeria* sp.) is a conserved PEP-utilizer superfamily domain, which exists as an extra C-terminal (CT) sequence. This finding suggested that some interaction could take place between PEP and the CT domain. This domain in *B. stearothermophilus* has been suggested to be derived from a PEP synthase late in the evolutionary process (*53*). However, the biological significance of this CT domain has not been fully elucidated. Since PKs from other sources lack the sequence, it is unlikely that it is essential for enzymatic activity or allosteric regulation. In this study, we examined in detail the influence of the CT domain on enzyme structure and function by characterizing a MRSA PK mutant (PK_{CT}) lacking the sequence. The expression level and the oligomeric state of the PK_{CT} were identical to those of the wild-type enzyme. The truncated enzyme exhibited PK activity similar to that of the wild-type protein, indicating that the CT domain is not essential for the activity or the allosteric nature of the enzyme. However, the $S_{0.5}$ values for PEP in the absence and presence of AMP and the concentration of AMP and R5P required for half-maximal activation of PK_{CT} were increased by 1.6-, 3.6-, 4.6-, and 24-fold (Tables 1 and 2), respectively, compared to the wild-type enzyme. Moreover, the stimulatory effect of low concentrations of ATP on enzyme activity was lost in PK_{CT}. These findings strongly suggest that potential interactions between the MRSA PK CT domain and the A and C domains may contribute to structural stability of the holomeric enzyme or to the specificity of the allosteric effectors of the enzyme, or both.

Sequence identity (68%), the presence of an extra C-terminal domain, kinetic properties, and mode of allosteric regulation of MRSA PK most closely resemble PK from *B. stearothermophilus*. Both MRSA and *B. stearothermophilus* PKs contain the CT domain and are regulated by AMP and R5P but not FBP and glucose 6-phosphate (*16*, *28*). However, CT truncation in *B. stearothermophilus* does not significantly alter the efficiency of the enzyme ($k_{cat}/S_{0.5}$) (*29*). In striking contrast, CT domain-deleted mutant MRSA PK exhibited dramatically lowered enzyme efficiency with $k_{cat}/S_{0.5}$ values less than 4.2% and 6.3% of those for PK_{WT} toward PEP and ADP, respectively, in the ligand-free state. However, enzyme efficiency of truncated MRSA PK was increased 3-fold in AMP-bound states, toward PEP. This increase in mutant enzymatic activity is most likely related to enhanced stability and rigidity of the protein upon effector binding. Such an effect has been previously reported for another CT-containing bacterial PK protein, *B. stearothermophilus* PK, as addition of the allosteric activator R5P resulted in a highly thermal stable PK conformation (*54*). These data are consistent with the potential requirement of CT domain interactions for optimal stability and rigidity of MRSA PK structure leading to efficient catalytic activity. This may involve enabling stronger interactions between adjacent domains of the tetramer, which are thought to be essential for subunit interactions. The recent crystal structure of *B. stearothermophilus* provided insight into the subunit interface between the CT domain and A domain of neighboring subunits. This appeared to involve the amide nitrogen of Leu_{538} in the CT domain of one subunit and the carboxyl oxygen of Glu_{209} in the A domain of the neighboring subunit to form a hydrogen bond (distance, 2.82 Å) in *B. stearothermophilus* PK (*6*). Leu_{538} and Glu_{209} in *B. stearothermophilus* PK are conserved as Leu_{536} and Glu_{207} in MRSA PK. The impact of the CT domain in stability and rigidity of the MRSA PK tetramer is of particular interest since the results of several published site-directed mutagenesis studies on PKs showed that single mutations located along the effector binding sites distant from the active sites can have unpredictably profound effects on the rates of enzyme catalysis. It is quite possible and highly likely that these effects may be due to altered dynamics of domains leading to possibly altered stability and rigidity of the tetramer (*1*, *55*−*58*). Nevertheless, the evolutionary advantage of the CT domain for *S. aureus* PK, if any, is not clear at this time. The PEP binding motif may participate in some as yet unknown enzymatic reaction. The possibility that the conserved histidine residues in the PEP-utilizer superfamily binding motif of MRSA PK are phosphorylated by PEP is, however, highly unlikely since it is replaced by proline at position 539 (Figure 1). The PEP binding motif may also participate in some as yet unknown enzymatic reaction.

The findings reported above provide novel insights into the functional features and mechanisms of regulation of *S. aureus* PK and its potential as an MRSA drug target. The essential nature of MRSA PK, the correlation of its peak enzymatic activity with exponential growth phase, its unique kinetic properties, and distinct allosteric regulation when compared with human isoforms suggest that it may be an attractive, novel drug target. This notion is supported further by the high level of sequence and structural divergence defined by biocomputational analysis between bacterial and mammalian PKs (Cherkasov et al., unpublished results). Currently, the availability of copious amounts of recombinant MRSA PK will facilitate both X-ray crystallographic studies aimed at the design of small molecules that selectively inhibit MRSA PK and screening of candidates in enzymatic assays.

ACKNOWLEDGMENT

Special thanks to Mrs. Marija Vuckovic from Dr. Natalie Strynadka's laboratory for help with size exclusion chromatography.

REFERENCES

1. Valentini, G., Chiarelli, L., Fortin, R., Speranza, M. L., Galizzi, A., and Mattevi, A. (2000) The allosteric regulation of pyruvate kinase. *J. Biol. Chem. 275*, 18145–18152.
2. Larsen, T. M., Laughlin, L. T., Holden, H. M., Rayment, I., and Reed, G. H. (1994) Structure of rabbit muscle pyruvate kinase complexed with Mn^{2+}, K^+, and pyruvate. *Biochemistry 33*, 6301–6309.
3. Jurica, M. S., Mesecar, A., Heath, P. J., Shi, W., Nowak, T., and Stoddard, B. L. (1998) The allosteric regulation of pyruvate kinase by fructose-1,6-bisphosphate. *Structure 6*, 195–210.
4. Speranza, M. L., Valentini, G., Iadarola, P., Stoppini, M., Malcovati, M., and Ferri, G. (1989) Primary structure of three peptides at the catalytic and allosteric sites of the fructose-1,6-bisphosphate-activated pyruvate kinase from *Escherichia coli*. *Biol. Chem. Hoppe-Seyler 370*, 211–216.
5. Rigden, D. J., Phillips, S. E., Michels, P. A., and Fothergill-Gilmore, L. A. (1999) The structure of pyruvate kinase from *Leishmania mexicana* reveals details of the allosteric transition and unusual effector specificity. *J. Mol. Biol. 291*, 615–635.
6. Suzuki, K., Ito, S., Shimizu-Ibuka, A., and Sakai, H. (2008) Crystal structure of pyruvate kinase from *Geobacillus stearothermophilus*. *J. Biochem. 144*, 305–312.
7. Stuart, D. I., Levine, M., Muirhead, H., and Stammers, D. K. (1979) Crystal structure of cat muscle pyruvate kinase at a resolution of 2.6 Å. *J. Mol. Biol. 134*, 109–142.
8. Valentini, G., Chiarelli, L. R., Fortin, R., Dolzan, M., Galizzi, A., Abraham, D. J., Wang, C., Bianchi, P., Zanella, A., and Mattevi, A. (2002) Structure and function of human erythrocyte pyruvate kinase. Molecular basis of nonspherocytic hemolytic anemia. *J. Biol. Chem. 277*, 23807–23814.
9. Munoz, M. E., and Ponce, E. (2003) Pyruvate kinase: current status of regulatory and functional properties. *Comp. Biochem. Physiol. B: Biochem. Mol. Biol. 135*, 197–218.
10. Noguchi, T., Inoue, H., and Tanaka, T. (1986) The M1- and M2-type isozymes of rat pyruvate kinase are produced from the same gene by alternative RNA splicing. *J. Biol. Chem. 261*, 13807–13812.
11. Dombrauckas, J. D., Santarsiero, B. D., and Mesecar, A. D. (2005) Structural basis for tumor pyruvate kinase M2 allosteric regulation and catalysis. *Biochemistry 44*, 9417–9429.
12. van Schaftingen, E., Opperdoes, F. R., and Hers, H. G. (1985) Stimulation of *Trypanosoma brucei* pyruvate kinase by fructose 2,6-bisphosphate. *Eur. J. Biochem. 153*, 403–406.
13. Iliffe-Lee, E. R., and McClarty, G. (2002) Pyruvate kinase from *Chlamydia trachomatis* is activated by fructose-2,6-bisphosphate. *Mol. Microbiol. 44*, 819–828.
14. Morgan, H. P., McNae, I. W., Nowicki, M. W., Hannaert, V., Michels, P. A., Fothergill-Gilmore, L. A., and Walkinshaw, M. D. (2010) The allosteric mechanism of pryuvate kinase from *Leishmania mexicana*: a rock and lock model, *J. Biol. Chem*. (in press).
15. Malcovati, M., and Valentini, G. (1982) AMP- and fructose 1,6-bisphosphate-activated pyruvate kinases from *Escherichia coli*. *Methods Enzymol. 90* (Part E), 170–179.
16. Sakai, H., Suzuki, K., and Imahori, K. (1986) Purification and properties of pyruvate kinase from *Bacillus stearothermophilus*. *J. Biochem. 99*, 1157–1167.
17. Chuang, D. T., and Utter, M. F. (1979) Structural and regulatory properties of pyruvate kinase from *Pseudomonas citronellolis*. *J. Biol. Chem. 254*, 8434–8441.
18. Crow, V. L., and Pritchard, G. G. (1982) Pyruvate kinase from *Streptococcus lactis*. *Methods Enzymol. 90* (Part E), 165–170.
19. Le Bras, G., and Garel, J. R. (1993) Pyruvate kinase from *Lactobacillus bulgaricus*: possible regulation by competition between strong and weak effectors. *Biochimie 75*, 797–802.
20. Kapoor, R., and Venkitasubramanian, T. A. (1983) Purification and properties of pyruvate kinase from *Mycobacterium smegmatis*. *Arch. Biochem. Biophys. 225*, 320–330.
21. Waygood, E. B., and Sanwal, B. D. (1974) The control of pyruvate kinases of *Escherichia coli*. I. Physicochemical and regulatory properties of the enzyme activated by fructose 1,6-diphosphate. *J. Biol. Chem. 249*, 265–274.
22. Opperdoes, F. R., and Michels, P. A. (2001) Enzymes of carbohydrate metabolism as potential drug targets. *Int. J. Parasitol. 31*, 482–490.
23. Christofk, H. R., Vander Heiden, M. G., Harris, M. H., Ramanathan, A., Gerszten, R. E., Wei, R., Fleming, M. D., Schreiber, S. L., and Cantley, L. C. (2008) The M2 splice isoform of pyruvate kinase is important for cancer metabolism and tumour growth. *Nature 452*, 230–233.
24. Vander Heiden, M. G., Christofk, H. R., Schuman, E., Subtelny, A. O., Sharfi, H., Harlow, E. E., Xian, J., and Cantley, L. C. (2010) Identification of small molecule inhibitors of pyruvate kinase M2. *Biochem. Pharmacol. 79*, 1118–1124.
25. Nowicki, M. W., Tulloch, L. B., Worralll, L., McNae, I. W., Hannaert, V., Michels, P. A., Fothergill-Gilmore, L. A., Walkinshaw, M. D., and Turner, N. J. (2008) Design, synthesis and trypanocidal activity of lead compounds based on inhibitors of parasite glycolysis. *Bioorg. Med. Chem. 16*, 5050–5061.
26. Chan, M., Tan, D. S., and Sim, T. S. (2007) Plasmodium falciparum pyruvate kinase as a novel target for antimalarial drug-screening. *Travel Med. Infect. Dis. 5*, 125–131.
27. Garcia-Lara, J., Masalha, M., and Foster, S. J. (2005) *Staphylococcus aureus*: the search for novel targets. *Drug Discovery Today 10*, 643–651.
28. Sakai, H., and Ohta, T. (1993) Molecular cloning and nucleotide sequence of the gene for pyruvate kinase of *Bacillus stearothermophilus* and the production of the enzyme in *Escherichia coli*. Evidence that the genes for phosphofructokinase and pyruvate kinase constitute an operon. *Eur. J. Biochem. 211*, 851–859.
29. Sakai, H. (2004) Possible structure and function of the extra C-terminal sequence of pyruvate kinase from *Bacillus stearothermophilus*. *J. Biochem. 136*, 471–476.
30. Yao, J., Zhong, J., Fang, Y., Geisinger, E., Novick, R. P., and Lambowitz, A. M. (2006) Use of targetrons to disrupt essential and nonessential genes in *Staphylococcus aureus* reveals temperature sensitivity of Ll.LtrB group II intron splicing. *RNA 12*, 1271–1281.
31. Branny, P., De La Torre, F., and Garel, J. R. (1993) Cloning, sequencing, and expression in *Escherichia coli* of the gene coding for phosphofructokinase in *Lactobacillus bulgaricus*. *J. Bacteriol. 175*, 5344–5349.
32. Branny, P., De La Torre, F., and Garel, J. R. (1996) The genes for phosphofructokinase and pyruvate kinase of *Lactobacillus delbrueckii* subsp. *bulgaricus* constitute an operon. *J. Bacteriol. 178*, 4727–4730.
33. Llanos, R. M., Harris, C. J., Hillier, A. J., and Davidson, B. E. (1993) Identification of a novel operon in *Lactococcus lactis* encoding three enzymes for lactic acid synthesis: phosphofructokinase, pyruvate kinase, and lactate dehydrogenase. *J. Bacteriol. 175*, 2541–2551.
34. Fraser, C. M., Gocayne, J. D., White, O., Adams, M. D., Clayton, R. A., Fleischmann, R. D., Bult, C. J., Kerlavage, A. R., Sutton, G., Kelley, J. M., Fritchman, R. D., Weidman, J. F., Small, K. V., Sandusky, M., Fuhrmann, J., Nguyen, D., Utterback, T. R., Saudek, D. M., Phillips, C. A., Merrick, J. M., Tomb, J. F., Dougherty, B. A., Bott, K. F., Hu, P. C., Lucier, T. S., Peterson, S. N., Smith, H. O., Hutchison, C. A., III, and Venter, J. C. (1995) The minimal gene complement of *Mycoplasma genitalium*. *Science 270*, 397–403.
35. Tanaka, K., Sakai, H., Ohta, T., and Matsuzawa, H. (1995) Molecular cloning of the genes for pyruvate kinase of two bacilli, *Bacillus psychrophilus* and *Bacillus licheniformis*, and comparison of the properties of the enzymes produced in *Escherichia coli*. *Biosci., Biotechnol., Biochem. 59*, 1536–1542.
36. Altschul, S. F., Gish, W., Miller, W., Myers, E. W., and Lipman, D. J. (1990) Basic local alignment search tool. *J. Mol. Biol. 215*, 403–410.
37. Forsyth, R. A., Haselbeck, R. J., Ohlsen, K. L., Yamamoto, R. T., Xu, H., Trawick, J. D., Wall, D., Wang, L., Brown-Driver, V., Froelich, J. M., C, K. G., King, P., McCarthy, M., Malone, C., Misiner, B., Robbins, D., Tan, Z., Zhu Zy, Z. Y., Carr, G., Mosca, D. A., Zamudio, C., Foulkes, J. G., and Zyskind, J. W. (2002) A genome-wide strategy for the identification of essential genes in *Staphylococcus aureus*. *Mol. Microbiol. 43*, 1387–1400.
38. Rodriguez, S. A., Davis, G., and Klose, K. E. (2009) Targeted gene disruption in *Francisella tularensis* by group II introns. *Methods 49*, 270–274.
39. Somerville, G. A., Chaussee, M. S., Morgan, C. I., Fitzgerald, J. R., Dorward, D. W., Reitzer, L. J., and Musser, J. M. (2002) *Staphylococcus aureus* aconitase inactivation unexpectedly inhibits post-exponential-phase growth and enhances stationary-phase survival. *Infect. Immun. 70*, 6373–6382.
40. Fry, B., Zhu, T., Domach, M. M., Koepsel, R. R., Phalakornkule, C., and Ataai, M. M. (2000) Characterization of growth and acid formation in a *Bacillus subtilis* pyruvate kinase mutant. *Appl. Environ. Microbiol. 66*, 4045–4049.
41. Abbe, K., and Yamada, T. (1982) Purification and properties of pyruvate kinase from *Streptococcus mutans*. *J. Bacteriol. 149*, 299–305.
42. Schaub, J., Schiesling, C., Reuss, M., and Dauner, M. (2006) Integrated sampling procedure for metabolome analysis. *Biotechnol. Prog. 22*, 1434–1442.
43. Bennett, B. D., Kimball, E. H., Gao, M., Osterhout, R., Van Dien, S. J., and Rabinowitz, J. D. (2009) Absolute metabolite concentrations and implied enzyme active site occupancy in *Escherichia coli*. *Nat. Chem. Biol. 5*, 593–599.

44. Asanuma, N., Kanada, K., and Hino, T. (2008) Molecular properties and transcriptional control of the phosphofructokinase and pyruvate kinase genes in a ruminal bacterium, *Streptococcus bovis*. *Anaerobe 14*, 237–241.
45. Kowalczyk, M., and Bardowski, J. (2007) Regulation of sugar catabolism in *Lactococcus lactis*. *Crit. Rev. Microbiol. 33*, 1–13.
46. Zhang, R., Ou, H. Y., and Zhang, C. T. (2004) DEG: a database of essential genes. *Nucleic Acids Res. 32*, D271–272.
47. Akerley, B. J., Rubin, E. J., Novick, V. L., Amaya, K., Judson, N., and Mekalanos, J. J. (2002) A genome-scale analysis for identification of genes required for growth or survival of *Haemophilus influenzae*. *Proc. Natl. Acad. Sci. U.S.A. 99*, 966–971.
48. Song, J. H., Ko, K. S., Lee, J. Y., Baek, J. Y., Oh, W. S., Yoon, H. S., Jeong, J. Y., and Chun, J. (2005) Identification of essential genes in *Streptococcus pneumoniae* by allelic replacement mutagenesis. *Mol. Cells 19*, 365–374.
49. Sassetti, C. M., Boyd, D. H., and Rubin, E. J. (2003) Genes required for mycobacterial growth defined by high density mutagenesis. *Mol. Microbiol. 48*, 77–84.
50. Thomson, C. J., Power, E., Ruebsamen-Waigmann, H., and Labischinski, H. (2004) Antibacterial research and development in the 21(st) century—an industry perspective of the challenges. *Curr. Opin. Microbiol. 7*, 445–450.
51. Cunningham, D. S., Liu, Z., Domagalski, N., Koepsel, R. R., Ataai, M. M., and Domach, M. M. (2009) Pyruvate kinase-deficient *Escherichia coli* exhibits increased plasmid copy number and cyclic AMP levels. *J. Bacteriol. 191*, 3041–3049.
52. Tulloch, L. B., Morgan, H. P., Hannaert, V., Michels, P. A., Fothergill-Gilmore, L. A., and Walkinshaw, M. D. (2008) Sulphate removal induces a major conformational change in *Leishmania mexicana* pyruvate kinase in the crystalline state. *J. Mol. Biol. 383*, 615–626.
53. Pocalyko, D. J., Carroll, L. J., Martin, B. M., Babbitt, P. C., and Dunaway-Mariano, D. (1990) Analysis of sequence homologies in plant and bacterial pyruvate phosphate dikinase, enzyme I of the bacterial phosphoenolpyruvate:sugar phosphotransferase system and other PEP-utilizing enzymes. Identification of potential catalytic and regulatory motifs. *Biochemistry 29*, 10757–10765.
54. Lovell, S. C., Mullick, A. H., and Muirhead, H. (1998) Cooperativity in *Bacillus stearothermophilus* pyruvate kinase. *J. Mol. Biol. 276*, 839–851.
55. Hannaert, V., Yernaux, C., Rigden, D. J., Fothergill-Gilmore, L. A., Opperdoes, F. R., and Michels, P. A. (2002) The putative effector-binding site of *Leishmania mexicana* pyruvate kinase studied by site-directed mutagenesis. *FEBS Lett. 514*, 255–259.
56. Ikeda, Y., Tanaka, T., and Noguchi, T. (1997) Conversion of non-allosteric pyruvate kinase isozyme into an allosteric enzyme by a single amino acid substitution. *J. Biol. Chem. 272*, 20495–20501.
57. Collins, R. A., Kelly, S. M., Price, N. C., Fothergill-Gilmore, L. A., and Muirhead, H. (1996) Ligand-induced conformational changes in wild-type and mutant yeast pyruvate kinase. *Protein Eng. 9*, 1203–1210.
58. Mattevi, A., Valentini, G., Rizzi, M., Speranza, M. L., Bolognesi, M., and Coda, A. (1995) Crystal structure of *Escherichia coli* pyruvate kinase type I: molecular basis of the allosteric transition. *Structure 3*, 729–741.
59. Dereeper, A., Guignon, V., Blanc, G., Audic, S., Buffet, S., Chevenet, F., Dufayard, J. F., Guindon, S., Lefort, V., Lescot, M., Claverie, J. M., and Gascuel, O. (2008) Phylogeny.fr: robust phylogenetic analysis for the non-specialist. *Nucleic Acids Res. 36*, W465–469.